Applied Catalysis A, General 682 (2024) 119799

Contents lists available at ScienceDirect

Applied Catalysis A, General

journal homepage: www.elsevier.com/locate/apcata

One-pot CO_2-to-olefins via methanol over In_2O_3-ZrO_2/SAPO-34 catalysts mixtures with different spatial arrangements

Alessandro Porta [a], Chiara Coffano [a], Mattia Piacentini [a], Francesca Rabino [b], Barbara Picutti [c], Luca Lietti [a,*], Carlo Giorgio Visconti [a,*]

[a] Dipartimento di Energia, Politecnico Di Milano, via Lambruschini 4, Milano 20156, Italy
[b] NextChem Tech S.p.A. (Maire Tecnimont Group), via di Vannina 88/94, Roma 00156, Italy
[c] Tecnimont S.p.A. (Maire Tecnimont Group), Via Gaetano de Castilla 6/A, Milano 20124, Italy

ARTICLE INFO

Keywords:
CCU
CO_2 hydrogenation
Lower olefins
Indium
SAPO-34
Deactivation

ABSTRACT

The one-pot CO_2 hydrogenation to lower olefins involves the integration of two catalytic reactions in a single reactor: the conversion of CO_2 into methanol (CTM) and its subsequent conversion into lower olefins (MTO). This approach requires two catalysts cooperating in the same reactor, posing different challenges in terms of synergies and interactions between the two active phases. In this work, we investigate the effect of process conditions and arrangements between In_2O_3-ZrO_2 (CTM catalyst) and SAPO-34 (MTO catalyst) on the lower olefins yield. We show that the distance between CTM and MTO active sites, studied by assessing different catalyst arrangements spanning from an intimate mixture obtained through mortar mixing to a complete segregation of the catalysts (i.e., consecutive beds), plays a key role in driving the products distribution. However, the thermodynamic equilibrium of the reverse water gas shift limits CO_2 conversion in the investigated conditions. Finally, we discuss the stability of the catalytic performances: the characterization of the spent samples after ~400 h on stream indicated the deactivation of the catalytic materials in all investigated cases, with In sintering on the methanol catalyst, and SAPO-34 losing both P and Al due to hydrothermal aging; indications of In migration on SAPO-34 were also observed when the two catalyst are in contact.

1. Introduction

The utilization of captured CO_2 as a feedstock for producing chemicals not only helps to reduce the effect of anthropogenic carbon emissions [1], but also offers a sustainable solution to replace fossil fuel reserves, since CO_2 can be considered as an economical, safe, and renewable carbon source [2–5]. Among Carbon Capture and Utilization (CCU) technologies, the conversion of CO_2 into value-added chemicals, such as lower olefins ($C_2^=$-$C_4^=$, i.e., ethylene, propylene, and butylene) is particularly appealing. In fact, lower olefins are key building blocks of the chemical industry and are traditionally produced by fossil resources with energy intensive processes such as steam cracking [6].

CO_2 can be converted to lower olefins according to two main routes, i.e. the Fischer-Tropsch (FT) route or the MeOH-mediated route. This work focuses on the CO_2-to-olefins process (CTO) following the one-pot methanol-mediated route, in which two consecutive reaction steps occur in the same reactor [7]: CO_2 is hydrogenated to methanol (CO_2-to-methanol, CTM, Eq. 1), which is then converted into hydrocarbons, through the methanol-to-olefins reaction (MTO, Eq. 2).

$$\text{CTM}: \quad CO_2 + 3H_2 \rightarrow CH_3OH + H_2O \tag{1}$$

$$\text{MTO}: \quad nCH_3OH \rightarrow C_nH_{2n} + nH_2O \tag{2}$$

The reverse water gas shift reaction (RWGS, Eq. 3) is also inevitably occurring in the reaction environment, leading to the production of CO, which can also react further to produce methanol, as its reactivity is higher than that of CO_2 [8,9].

$$\text{RWGS}: \quad CO_2 + H_2 \rightarrow CO + H_2O \tag{3}$$

Coupling the CTM and MTO processes is challenging. Indeed, the methanol formation is an equilibrium-limited exothermic reaction that occurs with a decreasing number of moles; thus, it is favored at low temperatures and high pressures [10]. In contrast, the MTO reaction is under kinetic control and is conducted industrially at high temperatures and low pressure [11]. Accordingly, it is critical to find a balance in the operating conditions to obtain good activity and minimize the selectivity

* Corresponding authors.
E-mail addresses: luca.lietti@polimi.it (L. Lietti), carlo.visconti@polimi.it (C.G. Visconti).

https://doi.org/10.1016/j.apcata.2024.119799
Received 4 February 2024; Received in revised form 22 April 2024; Accepted 10 May 2024
Available online 15 May 2024

to by-products, particularly CO formed through the thermodynamically favoured RWGS at the temperatures required by the MTO reactivity. In addition, the high partial pressure of hydrogen decreases the olefins to paraffins ratio (O/P) with respect to conventional MTO, carried out in the absence of H_2 and at low pressure [12].

Typically, the employed catalytic systems combine a methanol synthesis catalyst (mixed-metal oxides) and a zeolite for methanol conversion into olefins. Beyond activity and selectivity, these catalysts should demonstrate stability [13].

The limited stability at high temperatures of the well-known CZA catalyst (Cu-ZnO-Al_2O_3) for methanol synthesis [14], stimulated the research of alternatives. Several metal-oxide based catalysts have gained attention in the literature [15,16]. Among them, In_2O_3-based catalysts have demonstrated promising performances in the CO_2 hydrogenation to MeOH [14]. However, In_2O_3 has proven to be susceptible to sintering at the high temperatures required for the one-pot CTO process, resulting in a loss of catalytic activity during time on stream [17]. A possible solution involves stabilizing In_2O_3 with ZrO_2: when prepared by co-precipitation, mixed indium-zirconium oxides show high stability [17] and high activity [18] in the CO_2 conversion to methanol, thanks to the ability of ZrO_2 to prevent In_2O_3 sintering while generating more oxygen vacancies at the same time, which increases CO_2 adsorption and its subsequent hydrogenation [19].

The MTO process is conducted industrially over SAPO-34, a silicoaluminophospate zeolite with a chabazite (CHA) framework, which ensures very high lower olefins selectivity thanks to its moderate acidity and specific topology, with large cages and narrow windows [20]. Although the mechanism for olefins formation in the MTO reaction is still under debate, a consensus exists regarding a dual cycle mechanism. According to this mechanism, which is influenced by the zeolite topology, the products may be formed by an alkene or aromatic-based cycle via continuous methylation/cracking reaction of the formed intermediates [21]. The accumulation of polycyclic aromatics makes SAPO-34 susceptible to deactivation at the typical conditions of industrial MTO [20]. However, it has been speculated that the high partial pressure of hydrogen used in CTO process inhibits the formation of polycyclic aromatic species on the zeolite, thus slowing down catalyst deactivation [20,22]. Water also plays a key role in the stability of SAPO-34 [23]: it has been shown that it is able to reduce the growth rate of coke precursor species [23], thanks to its competitive adsorption onto the zeolite acid sites [20].

When the CTM and MTO catalysts are coupled in a single reactor, high temperatures and high pressures are needed to achieve relevant CO_2 conversion; however, under these conditions the RWGS becomes favoured and high CO selectivity is obtained [24]. Milder temperatures must be used to reduce CO selectivity, but at those conditions the CO_2 conversion reduces [25]. Moreover, the MTO chemistry imposes a lower boundary on the process temperature, as below 350 °C the hydrocarbon yield is severely hindered [26] and the catalyst quickly deactivates [27]. The O/P ratio depends much on the Gas Hourly Space Velocity (GHSV) [28,29], and by tuning the contact time between MeOH produced in the CTO reaction and the zeolite, the fraction of olefins in the hydrocarbon pool can be maximized.

The integration of the two processes in a single reactor also presents the opportunity to enhance MeOH synthesis by continuously removing the produced MeOH from the reaction environment, due to its conversion on the zeolite. In this regard, the spatial arrangements of CTM and MTO catalysts is expected to play a crucial role. One approach is to place the two catalysts in close intimacy ("intimate mixture"). To this aim, the two catalysts are crushed together in a mortar or in a ball-milling, thus allowing a close contact between the two active phases [30–33]. Another option is to individually pelletize the catalysts, gently mixing them before loading the reactor [29,34]: the obtained "mechanical mixture" avoids a close contact between the two active phases. In both cases, the contact between the catalysts presents some challenges, as the mobile indium species may migrate onto the zeolite acid sites, reducing the catalyst activity. This phenomenon has been reported both for the "intimate mixture" [35] and for the "mechanical mixture" [36]. A further increase of the distance between active phases can be obtained by adopting two catalysts bed in series ("consecutive beds"). This solution, however, has been shown to lead to diminished performances [29]. In addition to these effects, the selectivity towards the products depends on the relative amount of the CTO catalyst with respect to the MTO catalyst, that is on the residence time of the reaction intermediates in the presence of the two catalysts [32,34]. In any configuration, a diluent can be also added to the two catalysts to tune the average distance among the active sites.

Starting from the results of our previous publication [26], in this study we have further investigated the strategies for tuning the selectivity of the one-pot hydrogenation of CO_2 to lower olefins. Initially, we have studied the effect of variations in pressure and space velocity on the performances of a In_2O_3-ZrO_2 + SAPO-34 system, considering the reference case of a mechanical mixture and comparing it to the performance obtained when testing two consecutive beds. The spent materials were characterized in both cases, to gain insights on the possible causes of loss of performance during the direct hydrogenation of CO_2 to lower olefins. Subsequently, we have investigated the effects of the interaction between the two catalytic materials. To this aim, various catalyst arrangements were explored, progressively reducing the distance between the active phases: separated consecutive beds, diluted mechanical mixture, mechanical mixture, and intimate mixture. On the mechanical mixture, we have also studied the effect of the relative amount of In_2O_3-ZrO_2 and SAPO-34 catalysts.

2. Experimental

2.1. Materials

The home-made In_2O_3-ZrO_2 (In:Zr = 1:1, molar basis) was prepared by coprecipitation in a jacketed reactor according to the recipe provided in [19]. In the same work, the authors report that the material with In:Zr = 1:1 molar ratio shows the highest methanol yield, and hence was taken as reference material. Hydrated $In(NO_3)_3$ (Thermo Fischer Scientific, 99.99% metals basis) and $ZrO(NO_3)_2$ (Alfa Aesar, 99.9% metals basis) were dissolved in deionized water. Separately, the precipitating solution was prepared by mixing NH_4OH (32 wt% in H_2O, Merck) and ethanol (anhydrous, Carlo Erba Reagents) in a 1:3 ratio by volume, to obtain a double volume of precipitating solution with respect to the mother solution. The former was then added to the latter with a fixed rate of 2.5 mL/min, at room temperature and under stirring. Once the precipitating solution had been consumed, the slurry reached pH = 10, and it was heated at 80 °C (heating rate: 3 °C/min) and kept for 30 min under stirring. The precipitate was then filtered from the mother liquor using a filter press and washed with deionized water until neutral pH was measured in the washing solution. The obtained white solid was dried at 65 °C overnight and calcined in static air at 500 °C (heating rate: 2 °C/min) for 3 h.

A commercially available SAPO-34 sample was purchased from ZR Catalyst. The zeolite was calcined for 5 h at 550 °C before its use.

Each sample was pressed into tablets, grinded and sieved to obtain a particle size between 106 and 125 μm (120–140 mesh) before catalytic tests. Experiments with diluted catalyst bed have been carried out using low surface area α-Al_2O_3 (SASOL Puralox) also sieved in the range 106 – 125 μm.

2.2. Materials characterization

The fresh and spent catalysts were analyzed using different techniques. The textural properties of the samples were investigated by N_2 adsorption-desorption at 77 K to estimate the specific surface area and pore volume of the catalysts (BET analysis), using a Micromeritics Tristar 3000 instrument. The average pore diameter was evaluated from

the adsorption branch of the isotherm using the BJH method. XRD patterns were obtained using a Panalytical Empyrean diffractometer, using a Cu-Kα radiation source. A scanning electron microscope (SEM) (Zeiss Sigma 500) equipped with an energy dispersive X-ray spectrometer (EDS) (Oxford Ultim Max 65 Aztec Energy Advanced) was used to obtain images of the catalysts surfaces and their composition with an acceleration voltage of 20 kV. EDS quantitative data reported in this work are the averaged results of at least 10 measurements.

2.3. Catalytic activity tests

High pressure catalytic tests have been carried out in a fixed bed stainless steel (AISI 316 L) reactor with an internal diameter of 1.1 cm, located inside an electrical tubular oven. The catalysts were pre-treated in 9 L(STP)/h of 20% H_2/N_2 (molar basis) at 400 °C (heating rate: 2 °C/min) for 15 h. From there the temperature was lowered to 320 °C before feeding the H_2/CO_2 mixture ($H_2/CO_2/Ar$ = 73.5/24.5/2 molar basis) and increasing the pressure at 6 barg/h until the pressure of 38 barg (barg: relative pressure). The temperature was then increased to 380 °C (heating rate: 1 °C/min) and ToS (i.e., Time on Stream) was conventionally set at 0 h once the temperature of 380 °C was reached. Experiments have been carried out by varying the amounts and disposition of In_2O_3-Zr_2O and SAPO-34 inside the packed bed, as well as the pressure and the GHSV. All the GHSV values provided in this paper refer to the sole amount of methanol catalyst (In_2O_3-Zr_2O).

The effluent gases exiting the reactor were sent to a cold trap kept at 1 °C to remove water and methanol before the on-line compositional analysis. Condensable products were analyzed periodically using an off-line gas chromatograph (Hewlett-Packard 6890) equipped with a HP-5 crosslinked 5% PH ME Siloxane capillary column in He connected to a FID. Gaseous effluents were analysed on-line using a gas chromatograph (Hewlett-Packard 6890) equipped with: a molesieve 5 A connected to a TCD for the quantification of H_2, Ar, CH_4 and CO; a PorapakQ connected to a TCD for the quantification of CH_4, CO_2, and C_2–C_3 hydrocarbons, an Al_2O_3-plot capillary column connected to a FID for the analysis of C_1–C_7 hydrocarbons. In all the columns, He was used as carrier gas.

CO_2 conversion and C-selectivity are calculated according to Eqs. (4) and (5), respectively.

$$CO_2 \text{ conversion}: \quad \chi_{CO_2} = 1 - \frac{F_{CO_2}^{OUT}}{F_{CO_2}^{IN}} \tag{4}$$

$$C - \text{selectivity}: \quad \sigma_i = \frac{F_i^{OUT} \times nC_i}{F_{CO_2}^{IN} - F_{CO_2}^{OUT}} \tag{5}$$

Where F_i indicates the molar flowrate of the i-th species at the inlet or outlet, as indicated by the superscript notation, and nC_i indicates the number of carbon atoms of the i-th species. The molar flowrates at the outlet were evaluated from on-line GC measurements by using Ar as internal standard. H_2O and, if any, CH_3OH were condensed before the on-line analysis and their outlet flowrates were estimated periodically by the integral amount of product in the cold separator. In order to increase the number of H_2O flowrate data at the reactor outlet, a theoretical H_2O flowrate was calculated through the oxygen balance given the CO_2 conversion and product distribution, according to Eq. (6):

$$F_{H_2O}^{OUT} = \left(F_{CO_2}^{IN} - F_{CO_2}^{OUT}\right) \times 2 - F_{CO}^{OUT} - F_{CH_3OH}^{OUT} \tag{6}$$

The calculated and measured (integral) water production rates were always within 10% error.

2.4. Thermodynamic calculations

Thermodynamic equilibrium calculations were carried out using the Gibbs Reactor tool in Aspen Plus V10 while using the Peng-Robinson Equation of State and considering CO and CH_3OH as the only C-containing products.

The approach to equilibrium for the RWGS reaction was monitored by calculating the ratio between the reaction quotient (K_p) and the equilibrium constant (K_{eq}). The latter was computed based on thermodynamic data, while the former was computed according to Eq. (7):

$$K_p^{RWGS} = \frac{y_{CO}^{OUT} \times y_{H_2O}^{OUT}}{y_{H_2}^{OUT} \times y_{CO_2}^{OUT}} \tag{7}$$

where y_i^{OUT} represents the molar fraction of species i at the reactor outlet, evaluated as ratio between the molar flowrate of the i-th speces and the total flowrate at the reactor outlet.

3. Results and discussion

3.1. Characterization of the fresh catalysts

The coprecipitated In_2O_3-ZrO_2 catalyst shows a surface area of 96 m^2/g and a pore volume of 0.19 cm^3/g, with an average pore diameter of 60 Å. The commercial SAPO-34 zeolite has a surface area of 477 m^2/g, and pore volume of 0.31 cm^3/g. Additional characterization are shown and discussed in paragraphs 3.3 and 3.4, in comparison to those of the spent samples.

3.2. Activity and stability of the In_2O_3-ZrO_2/SAPO-34 systems

Fig. 1A shows the conversion and selectivity trends during more than 300 h on stream in the case of the mechanical mixture (MM) of In_2O_3-ZrO_2 and SAPO-34 catalysts in a 1:1 ratio by weight. Experiments have been carried out at the fixed temperature of 380 °C, i.e. at the optimal temperature identified in a previous study by some of us on the same MM [26]. CO_2 conversion increases during the first hours on stream at 38 barg and 3 L(STP)/h/g_{cat} and approaches the equilibrium conversion of 35% after about a day. The reaction products evolving from the catalyst show a slower transient, and steady state conditions are approached only after 100 h on stream. CO is always the most abundant product of this reaction, showing a decreasing trend in the first hours from 90% at ToS = 0 h to 60% at ToS = 20 h and then slowly increasing as ToS increases. In a specular fashion, lower paraffins (C_2°-C_4°) show a maximum at ToS = 20 h of 25% selectivity and then linearly decrease as ToS increases. Lower olefins ($C_2^=$-$C_4^=$) increase up to 15% selectivity at ToS = 20 h and then remain constant and parallel to the CO_2 conversion trend.

The paraffin formation during the initial induction time can be explained by considering the aromatic species formation within the zeolite. In fact, once the temperature is sufficiently high for the MTO reactivity to begin, the olefin aromatic species formation is expected within the zeolite cages, as a result of the condensation of olefins with the consequent elimination of a paraffin [21]. When experimental conditions are changed (GHSV in the range 3–9 L(STP)/h/gcat and P in the range 20–38 barg) the system response is faster if compared to the first condition. This is likely because the zeolite cages are already filled with aromatic species, effectively shortening the required induction time.

Fig. 2A and 2B summarizes the effects of pressure and GHSV, respectively, on CO_2 conversion and product selectivity when using the MM of In_2O_3-ZrO_2 and SAPO-34. Averaged data have been collected after at least 10 h spent at the same process condition, once stable performances have been recorded.

Increasing the pressure from 20 to 38 barg causes an increase in CO_2 conversion from 30% to 35%, coupled by a marked decrease of CO selectivity from 84% to 60% (Fig. 2A). This is attributed to the competition between the RWGS and methanol synthesis reaction. In fact, high pressures are required from a thermodynamic standpoint in order to obtain a reasonable methanol production at the relatively high temperatures required by the MTO reaction. As a result, upon increasing

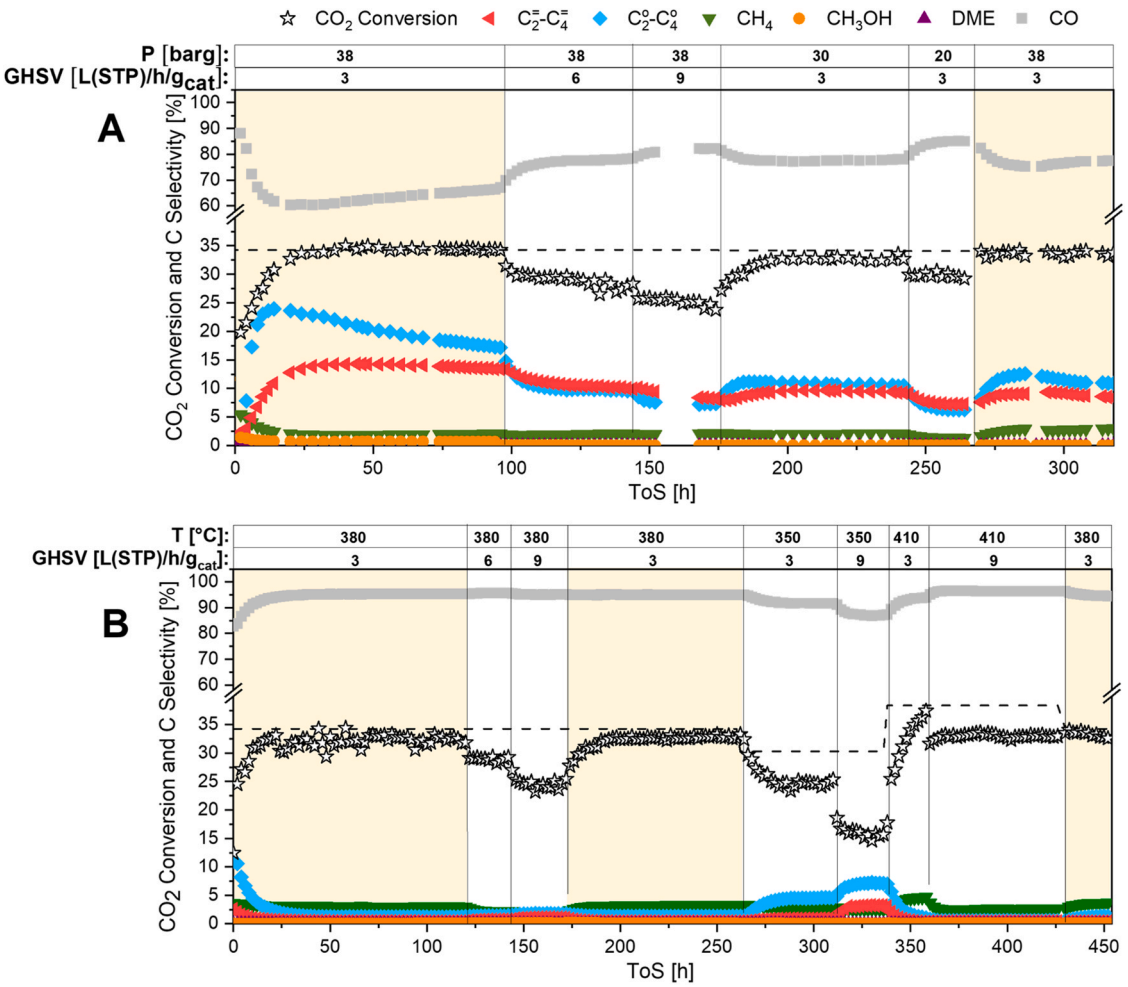

Fig. 1. CO_2 conversion, product selectivity (C-basis) trends as a function of ToS for: A) 2 g In_2O_3-ZrO_2 + 2 g SAPO-34 mechanical mixture (1:1 wt ratio) B) 2 g In_2O_3-ZrO_2 and 2 g SAPO-34 consecutive beds (1:1 wt ratio). Equilibrium conversion as a dotted line. Constant experimental conditions: A) T = 380 °C, H_2/CO_2=3/1 molar basis; B) P = 38 barg, H_2/CO_2= 3/1 molar basis. Experimental conditions varied in each run are reported in the table above each panel. Control points at the same experimental conditions are highlighted by yellow areas.

pressure, the production of hydrocarbons also increases significantly. However, increasing the pressure affects the hydrocarbon distribution in a negative way, as the olefin/paraffin ratio nearly halves passing from 20 to 38 barg. This could be ascribed to the complex interplay of hydrogen transfer and olefin hydrogenation reactions that can occur at these conditions.

Fig. 2A also shows the Kp/Keq ratio evaluated for the RWGS as indicated in the experimental section to quantify the approach to equilibrium of the RWGS reaction. At the pressure of 38 barg the RWGS is fully equilibrated (Kp/Keq = 1) and the global CO_2 conversion matches well with the thermodynamic equilibrium calculations (see Fig. 1A, ToS 50–100 h). As the pressure decreases a decrease in the Kp/Keq ratio is observed, indicating that the RWGS reaction is no longer equilibrated, coupled with a decrease in CO_2 conversion. Since pressure has no effect on the equilibrium composition of the RWGS, this can be explained with a kinetic effect: the rate of the RWGS decrease upon decreasing pressure, preventing the reaction to reach chemical equilibrium.

Considering the GHSV effect (Fig. 2B) at the constant pressure of 38 barg, increasing the GHSV from 3 to 9 L(STP)/h/g has an opposite effect to those observed in Fig. 2A while increasing the pressure. In fact, increasing the GHSV has a negative effect on the slow CTM step, moving the CO_2 conversion away from the equilibrium at 35 down to 25%, and increasing CO selectivity from 60% to 82% at 3 and 9 L(STP)/h/g, respectively. Conversely, the O/P ratio grows upon increasing GHSV (i.e., at shorter contact times). In fact, the fast MTO step is able to fully convert all the produced methanol, and the secondary reactions bringing to olefins consumption (olefins hydrogenation and hydrogen transfer reactions) are occurring to a lower extent [37]. Interestingly, CH_4 selectivity remains almost unaffected when varying pressure and GHSV, remaining always below 5%.

The Kp/Keq ratio for the RWGS at different GHSV is also shown in Fig. 2B. Also in this case the trend of the Kp/Keq closely follows the CO_2 conversion trend, with both parameters decreasing as the GHSV increases. While at 3 L(STP)/h/g the RWGS kinetic is fast enough to reach fully equilibrated conditions, as the GHSV is increased to 6 and 9 L(STP)/h/g the contact time is progressively decreased and is not sufficient to reach chemical equilibrium for the RWGS reaction.

A similar run performed on the same amounts of In_2O_3-ZrO_2 and SAPO-34 but in a different spatial arrangement is shown in Fig. 1B. In this run the two materials were kept completely segregated using a layer of quartz wool, with the In_2O_3-ZrO_2 layer first, followed by the SAPO-34 layer. This configuration will be addressed throughout this work as "consecutive beds" configuration (CB). In this case the initial transient is much shorter, with paraffins and olefins monotonically decreasing as CO selectivity increases to 95%. Interestingly, the CO_2 conversion approaches 35% as predicted by thermodynamics and as obtained in the case of the MM, but in the presence of a completely different product distribution. In this case, also the CO selectivity is well in line with the equilibrium selectivity evaluated at this process conditions when considering CO and CH_3OH as the only C-containing products

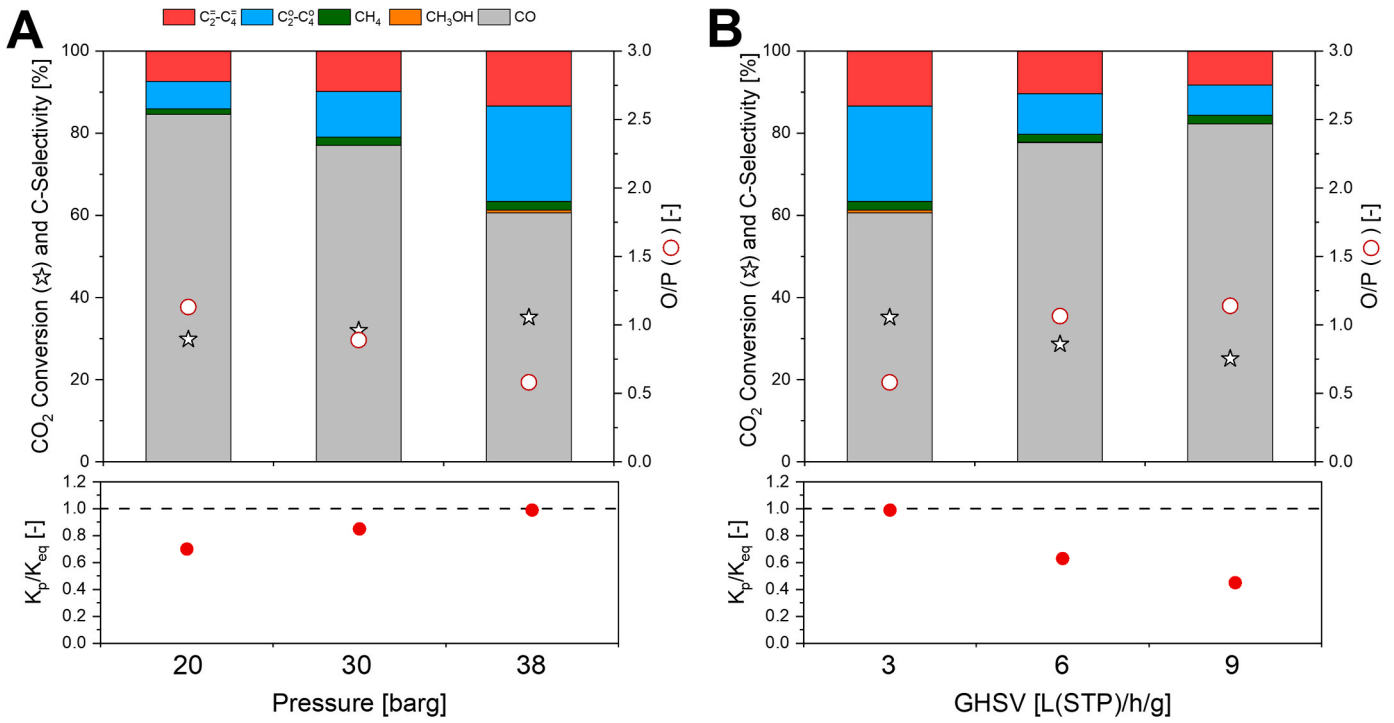

Fig. 2. . (A) Pressure effect at fixed GHSV = 3 L(STP)/h/g and (B) GHSV effect at fixed P = 38 barg on CO_2 conversion (star), product selectivity (C-basis, bars) and olefin/paraffin ratio (O/P, dot) on the In_2O_3-ZrO_2/SAPO-34 mechanical mixture (1:1 wt). For each condition, the ratio between the Kp and Keq of the RWGS equation is also shown. Fixed experimental conditions: $H_2/CO_2/Ar$ = 73.5/24.5/2, molar basis, T = 380 °C. The same effects are shown in Fig. 1A as a function of ToS.

(equilibrium calculations results are showed in Fig S1 of the Supporting Material), indicating that the system is fully equilibrated at the outlet of the In_2O_3-ZrO_2 layer, before entering in the SAPO-34. The effect of different catalytic arrangements on the product distribution will be deepened and discussed in Sections 3.5 and 3.6.

The GHSV (Fig. 1B, ToS = 120–175 h) as well as the T (Fig. 1B, ToS = 260 – 430 h) were varied in order to try and increase the hydrocarbon production, But CO selectivity was higher than 85% in all investigated conditions, with CH_4 or C_2-C_4 paraffins as second most abundant product. In the presence of high CO partial pressures olefins secondary hydrogenation can be effectively slowed down [22], but in this case the low methanol flowrate per zeolite mass is probably steering the selectivity of the process towards paraffins.

Both in the case of the MM and of the CB runs, control points were taken in the same reference conditions (GHSV = 3 L(STP)/h/g, T = 380 °C, P = 38 barg) to evidence variations in the system behavior. In the case of the MM (Fig. 1A), when the control point is replicated at ToS 270–320 h, the CO_2 conversion is still very close to the value predicted by thermodynamics, while the selectivity is changed: CO selectivity is higher, reaching 75%; and the O/P ratio is higher as well, getting close to 1. The replicated point seem to match well with the progression of the selectivity trends observed in the first 100 h on stream, suggesting a slow, but constant deactivation. In the case of the CB run (Fig. 1B) the replicated control points at ToS = 175 – 265 h and 430 – 450 h perfectly replicated the initial point in terms of conversion and selectivity. In fact, at these conditions the RWGS reaction is dominating, and closely approaching the thermodynamic equilibrium: this makes the identification of eventual differences in catalytic activity very challenging, and more information on the system stability can be obtained by characterizing the spent samples.

3.3. Characterization of the spent In_2O_3-ZrO_2

In order to rationalize the reasons behind the activity and selectivity change with ToS, the spent catalysts from the 1:1 mechanical mixture run (shown in Fig. 1A) and the spent catalysts from the consecutive beds run (shown in Fig. 1B) were characterized and compared with the fresh samples. XRD characterization on the spent materials form the MM test was carried out after mechanical separation of the two.

The XRD patterns of the fresh and spent In_2O_3-ZrO_2 are shown in Fig. 3.

The fresh In_2O_3-ZrO_2 sample shows the presence of cubic indium oxide and tetragonal zirconium oxide. The two metal oxides show their most intense diffraction features at similar angles, but from the magnification panel (Fig. 3B) it can be observed that the most intense feature in the case of the fresh sample falls at 2θ = 30.43°, which is midway from

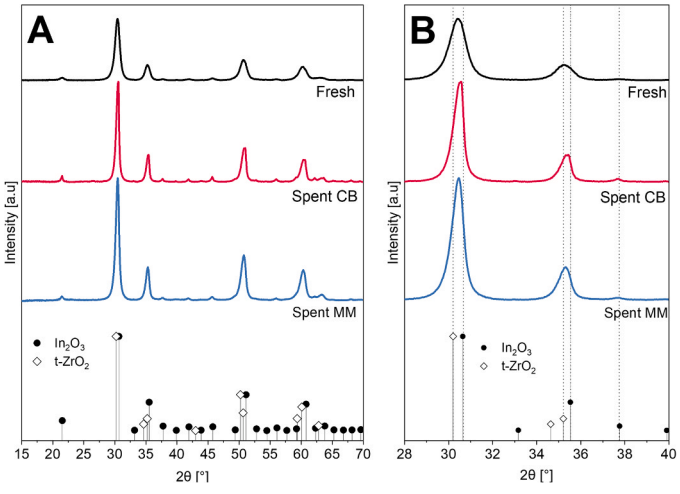

Fig. 3. . (A) Full XRD pattern and (B) magnification for the fresh In_2O_3-ZrO_2 (Fresh) and the spent In_2O_3-ZrO_2 taken from the 1:1 wt consecutive bed (Spent CB) and from the mechanical mixture (Spent MM). Reference patterns shown for cubic In_2O_3 (PANICSD: 98–025–2371) and tetragonal ZrO_2 (PANICSD: 98–015–7618).

the reference pattern of ZrO_2 and In_2O_3 ($2\theta = 30.22°$ and $30.64°$, respectively). This feature becomes sharper and leans toward In_2O_3 diffraction pattern in the case of the two spent samples, and especially in the spent In_2O_3-ZrO_2 from the consecutive beds test. This indicates a higher crystallinity of the indium phase on the spent samples, likely as a result of sintering phenomena.

To provide further data on catalyst deactivation, SEM-EDS analyses were performed on the same samples. Since the In_2O_3-ZrO_2 and SAPO-34 can be clearly identified, SEM imaging was performed on the mechanical mixture of the two materials without additional separation. The results are shown in Fig. 4.

The fresh In_2O_3-ZrO_2 sample (Fig. 4A) appears homogenous and spotless. EDS analysis on the fresh sample indicated an atomic In/Zr ratio of 0.98 ± 0.03 (see Fig S2 in the Supporting Material for additional SEM imaging and indication of the areas where the composition was measured), well in line with the theoretical value of 1. The homogeneity of the sample can be observed from the In and Zr maps (Figs. 4B and 4C, respectively) where both metals appear well distributed. The smaller bits visible on the particle do not show compositional differences, and are likely the outcome of the pelletization, crushing and sieving procedure of the coprecipitated sample.

The spent sample coming from the MM run (reported in Fig. 1A) is shown in Fig. 4D, with In and Zr maps in Figs. 4E and 4F, respectively. In this case EDS mapping reveals a pronounced In spot in the center, where Zr is absent and crystals are evident, together with In-enriched areas on the pellet surface, without the evident formation of crystals. Note that the well-defined cubic crystallites shown in the spent sample from the MM (Fig. 4D-F) in fact are SAPO-34 crystallites as indicated by the Al signal from EDS (see Supporting Material, Fig S3). The spent sample from the CB run (reported in Fig. 1B), is shown in Fig. 4G, with In and Zr maps in Figs. 4H and 4I, respectively. Circular spots made of cubic In_2O_3 crystals are more evident on the surface of this In_2O_3-ZrO_2 sample, and also outside of the In spots, EDS measurements indicated an In enrichment of the surface with respect to the fresh sample, yielding a In/Zr atomic ratio of 1.4 ± 0.2 (see Supporting Material, Fig S4 and S5).

These results clearly indicate that indium oxide is sintering at CTO conditions [17]. The more pronounced sintering in the case of the spent In_2O_3-ZrO_2 from the CB run could be attributed to the higher temperature reached during the run in the presence of H_2/CO_2 (410 °C) with respect to the MM run (380 °C).

3.4. Characterization of the spent SAPO-34

The XRD characterization of the fresh and spent SAPO-34 samples is shown in Fig. 5.

The fresh SAPO-34 shows a well-defined chabazite structure. On the spent samples, the intensity of the main chabazite feature at $2\theta = 9.5°$ is decreased. Also the relative ratio of the peak is changing, for example the relative intensity of the peak at $2\theta = 9.5°$ compared to that at 13° drops from a value of 3 in the case of the fresh sample to 2.2 and 2.1 in the case of the spent SAPO-34 from the consecutive bed and mechanical mixture run, respectively. These data indicate a lower crystallinity and a possible modification of the chabazite structure at CTO process conditions. While, in the case of the consecutive beds run, the spent SAPO-34 is only showing a change in the diffraction pattern intensity, in the case of the spent SAPO-34 from the mechanical mixture the peaks are also

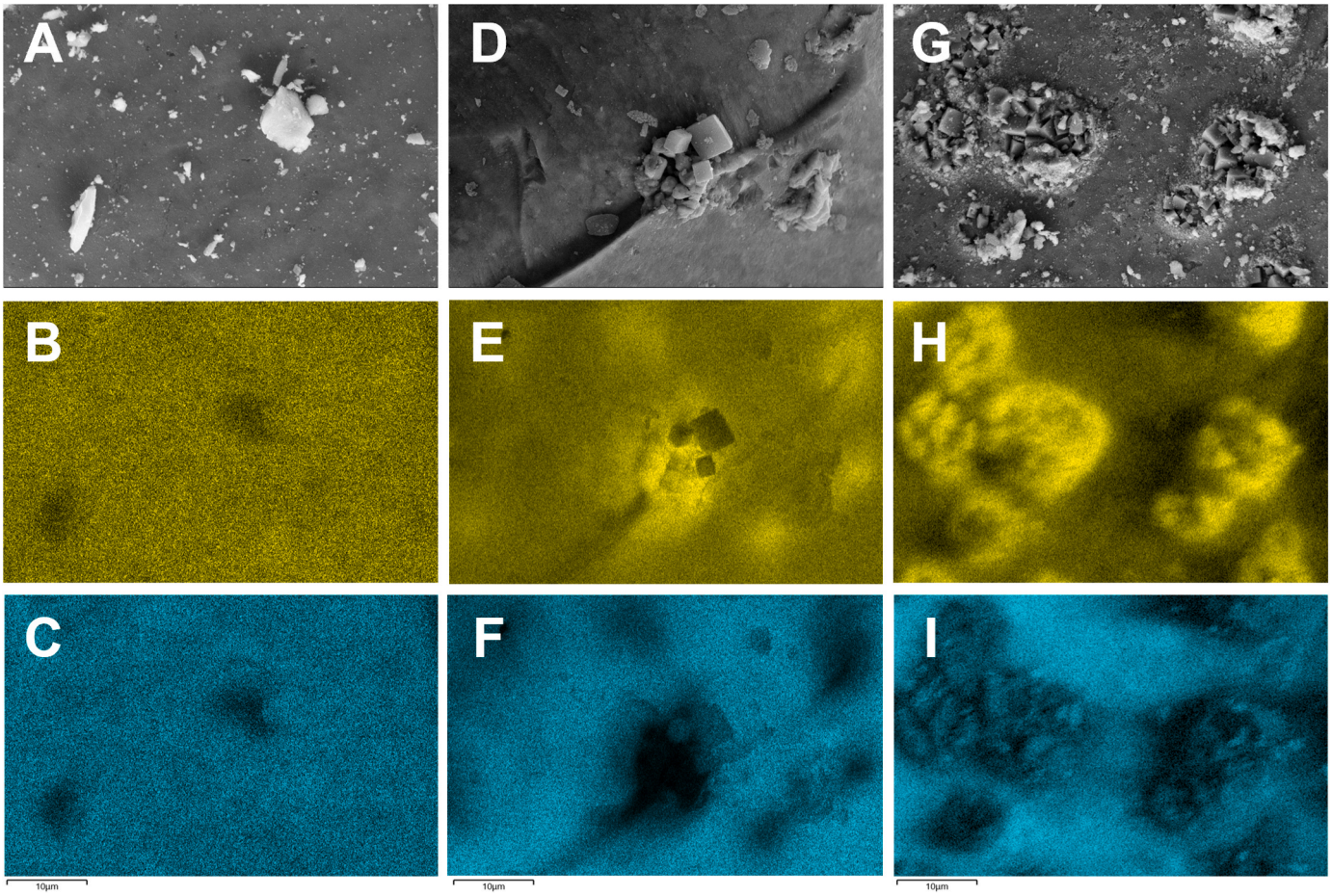

Fig. 4. SEM images of (A) fresh In_2O_3-ZrO_2 sample, (D) spent In_2O_3-ZrO_2 from the MM run shown in Fig. 1A, (G) spent In_2O_3-ZrO_2 from the CB run shown in Fig. 1B. Below each sample are shown the corresponding EDS maps highlighting In in yellow (B, E, H) and Zr in blue (C, F, I). All images are taken at 5000x magnification with EHT = 20 kV.

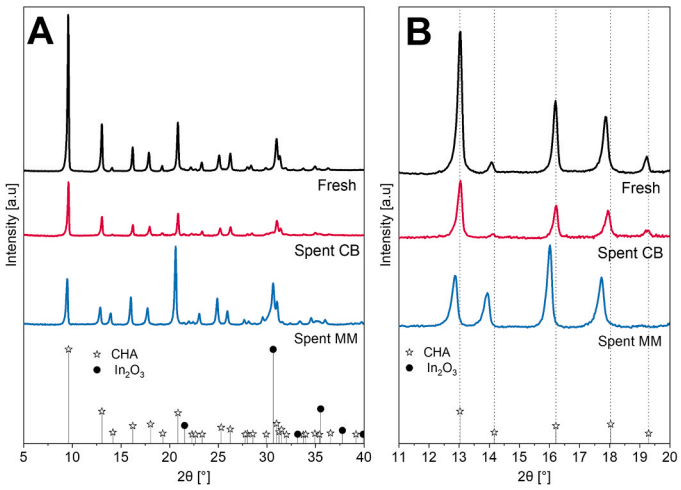

Fig. 5. . (A) Full XRD pattern and (B) magnification for the fresh SAPO-34 (Fresh) and the spent SAPO-34 taken from the 1:1 wt consecutive bed (Spent CB) and from the mechanical mixture (Spent MM). Reference patterns are shown for chabazite (PANICSD: 98–019–4279) and cubic In_2O_3 (PANICSD: 98–025–2371).

shifted towards lower 2θ (Fig. 5B). This suggests an expansion of the zeolite lattice: this behavior is typically observed when a different cation with a longer cation-oxygen bond is introduced in the framework. The decrease of the intensity of the SAPO-34 diffraction pattern was also correlated to a strong lattice distortion in the presence of water [38].

To further investigate the structural modifications of the spent SAPO-34, SEM images for the same samples are shown in Fig. 6A-C.

The fresh zeolite (Fig. 6A) shows cubic crystallites, with an average dimension of about 5 μm. The spent SAPO-34 from the mechanical mixture test (Fig. 6B) can retain its shape, while the spent sample from the consecutive bed run (Fig. 6C) shows a significant shattering of the zeolite cubes, with the formation of smaller particles of irregular shape.

The relative atomic ratio between the metals present in the samples is reported in Table 1. The reader is referred to the Supporting Material (Figs S5, S6, S7) for additional SEM images with the indication of the area where the EDS measurements were taken. The fresh sample shows similar contents of Al and P. On the contrary both spent samples show significantly lower values for the Al/Si and P/Si ratios, indicating the dealumination and dephosphoration of the SAPO-34 at CTO conditions. In the case of the spent SAPO-34 from the mechanical mixture, the loss of Al and P appears less evident, in agreement with the retention of the crystalline shape. It is speculated that the differences between the consecutive bed and mechanical mixtures depends on the different amount of methanol and water present in the reaction environment at CTO conditions. In the CB arrangement, the synergy between the two catalysts is low and only a little amount of MeOH is formed and subsequently converted into hydrocarbons. For these reasons, also H_2O concentration in the reactor is low. In contrast, the MM shows a positive synergy between the phases, enhancing the MTO reaction, which increases the amount of MeOH and water present in the reaction environment. It is known that high water partial pressure can slow down coke deposition with a beneficial effect on the stability of high pressure MTO [23]. However, the positive effect is somewhat mitigated since SAPO-34 are known to be susceptible to hydrothermal aging [39], leading to partial dealumiation and dephosporation, even in the case of MM.

Table 1
Comparison of the fresh and spent SAPO-34 samples in terms of relative atomic ratios between Al, P, In and Si from SEM-EDS measurements.

	Al/Si	P/Si	In/Si
Fresh	7.3 ± 0.3	7.6 ± 0.3	Not detected
Spent CB	3.5 ± 1.7	2.6 ± 1.4	Not detected
Spent MM	5.6 ± 0.6	4.7 ± 0.6	0.6 ± 0.2

Furthermore, EDS analyses show a significant presence of In in the spent zeolite from the MM. Similar observations were reported by Wang et al. [36] using H-ZSM5 as MTO catalyst. In particular, they speculate that indium can migrate on the surface of a H-ZSM-5 as a form of liquid metal, given the high mobility and its low melting point (156 °C). In the same work evidences of in-situ ionic exchange on In at the expenses of zeolite protons are also provided. The migration of Zr as well cannot be excluded, however its quantification from EDS is challenging due to significant overlapping with the more intense P features.

NH_3-TPDs were performed on the fresh and spent SAPO-34 samples to characterize the impact of the SAPO-34 Al and P loss on the acidic properties. All samples were pretreated in diluted O_2 at 600°C prior to NH_3 adsorption. The results and experimental details are given in the Supporting Material in Fig S8. Both spent SAPO-34 show a marked decrease in NH_3 adsorption capability when compared to the fresh sample. In particular, the spent material from the CB run shows a marked decrease in NH_3 adsorption, indicating a major acidity loss. These results are in line with the SEM-EDS measurements, where the CB suffered from a more severe dealumination and dephosphorization with respect to the MM.

3.5. *In_2O_3-ZrO_2 and SAPO-34 spatial arrangement effects*

Given the marked differences in product selectivity obtained when comparing the same amounts of In_2O_3-ZrO_2 and SAPO-34 as a Mechanical Mixture (MM) or fully segregated Consecutive Beds (CB) (Fig. 1), other arrangements of the same catalyst amounts were considered to deepen the effect of the interaction between the two catalytic materials. Two additional experiments have been carried out, always keeping constant the amount of In_2O_3-ZrO_2 (2 g) and SAPO-34 (2 g) in the reactor: in one case the mechanical mixture of the two catalyst was diluted with 2 g of inert α-Al_2O_3 (Diluted Mechanical Mixture, DMM), to increase the relative distance of the two catalysts; the interaction between the two phases was also increased by means of

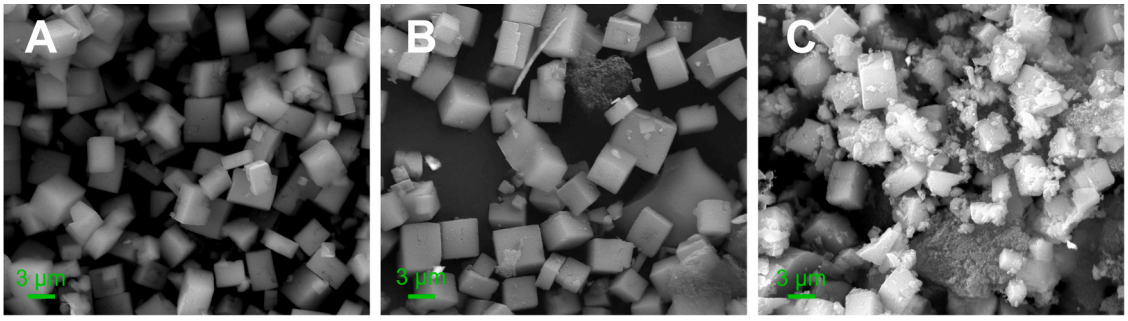

Fig. 6. SEM images of (A) the fresh SAPO-34 sample, (B) the spent SAPO-34 from the mechanical mixture run and from (C) the consecutive bed.

crushing in a mortar equal parts by weight of In_2O_3-ZrO_2 and SAPO-34, in order to obtain an Intimate Mixture (IM) of the two catalysts. The mortar mixing was carried out until both catalysts were crushed for few minutes to a homogeneous powder with average particle size below 75 μm (200 mesh). This powder was then pelletized, crushed and sieved to obtain particle diameters in the desired range 106–125 μm before catalytic tests.

The results obtained in these two additional arrangements are compared with the previously discussed MM and CB in Fig. 7, at the same process conditions and at comparable time on stream (T.o.S. = 60–90 h) in terms of CO_2 conversion and C-selectivity. For comparison's sake, the results obtained on the bare In_2O_3-ZrO_2 under the same conditions are also shown (labelled as Single Bed, SB).

As shown in Fig. 7, CO_2 conversion is not affected by the different catalysts arrangements, remaining always in the narrow range 32–35%. At variance, the arrangements of CTM and MTO catalysts have a strong impact on the product selectivity.

Starting from the most segregated system (consecutive bed configuration, CB column in Fig. 7), CO selectivity reaches values in excess of 95%, with nearly 3% selectivity to CH_4 and less than 2% of olefins and paraffins with two or more carbon atoms (C_{2+}). By comparing these results with those obtained in the case of the Single Bed of In_2O_3-ZrO_2 (SB column in Fig. 7), the CO_2 conversion and CO selectivity remains unchanged, with similar selectivity towards CH_4. The only difference between the two is the presence of methanol, which is measured at the outlet of the SB but is effectively converted to paraffins and olefins when SAPO-34 is located downstream (CB). These results are well in line with the thermodynamic equilibrium composition when only CO and CH_3OH are considered as C-containing products (98.5% CO and 1.5% CH_3OH, see Fig S1 in the Supporting Material). At the thermodynamic equilibrium in these conditions, given the relatively high T required by the MTO reaction, CO formation via RWGS is predominant with respect to methanol formation. By computing the ratio between the reaction quotient Kp and equilibrium constant Keq when considering the RWGS reaction as detailed in the experimental section, values approaching 1 are obtained in both cases. Accordingly, we can conclude that at these process conditions the system is equilibrated at the outlet of the In_2O_3-ZrO_2 bed and remains equilibrated as the produced methanol is fully converted into paraffins and olefins on the subsequent SAPO-34. However, because of the very low methanol to H_2 ratio at the inlet of the SAPO-34 bed, hydrogen transfer reactions [40] and secondary hydrogenation of the produced olefins can significantly occur [12], leading to a low olefin selectivity (O/P ratio close to 0.3).

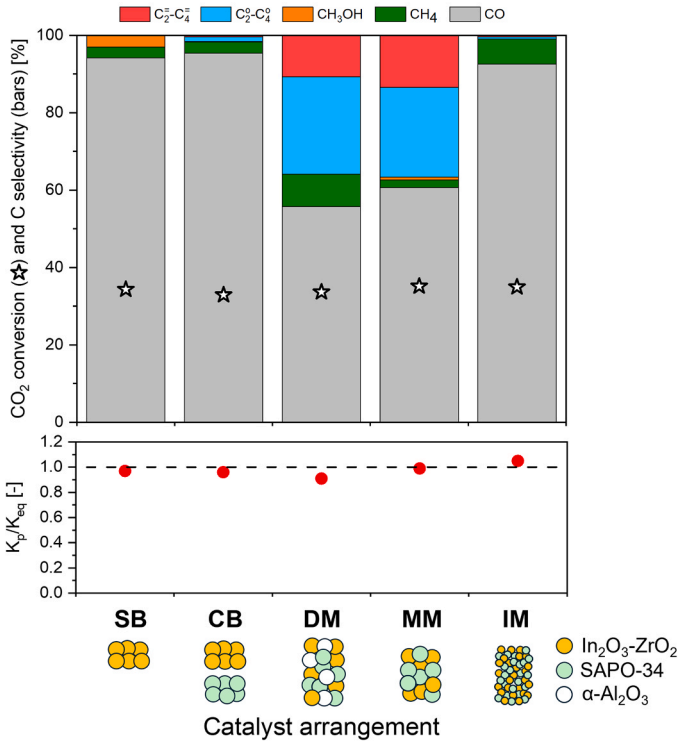

Fig. 7. CO_2 conversion and products C-selectivity obtained with different arrangements of In_2O_3-ZrO_2/SAPO-34 (1:1 wt). CB = Consecutive Beds, In_2O_3-ZrO_2 first and SAPO-34 after; DMM = Diluted Mechanical Mixture, with inert α-Al_2O_3; MM = Mechanical Mixture; IM = Intimate Mixture, obtained via mortar mixing. The results obtained in the case of the sole In_2O_3-ZrO_2 (SB = Single Bed) are also shown. For each configuration, the ratio between the Kp and Keq of the RWGS equation is also shown. Experimental conditions: H_2/CO_2/Ar = 73.5/24.5/2 molar basis, T = 380 °C, P = 38 barg, GHSV = 3 L(STP)/h/g, Flowrate = 6 L(STP)/h.

At variance, when the catalysts are mixed together (MM in Fig. 7) a marked increase in the hydrocarbon selectivity at the expense of CO is observed, testifying a synergistic effect when the two phases are in contact. In fact, the zeolite is able to quickly remove methanol from the reaction environment, effectively pushing methanol formation. However, while the effect on selectivity is remarkable, the CO_2 conversion is almost the same between the DB and MM configuration. In both conditions the Kp/Keq ratio for the RWGS at the outlet of the catalyst bed yields a perfectly equilibrated value of 1. These observations indicate that the thermodynamic equilibrium of the RWGS reaction is limiting the overall CO_2 conversion: in fact, at the investigated conditions the RWGS kinetic rate is fast enough to restore the thermodynamic equilibrium composition (i.e., the methanol formation/consumption reaction is not fast enough to pull away the outlet concentration from the thermodynamic equilibrium), thus preventing additional CO_2 conversion despite the increased methanol consumption. Since every mol of CH_3OH converted into hydrocarbons leads to the formation of a mol of H_2O, this contributes to the maintenance of the equilibrium and constant CO_2 conversion [26].

Upon increasing the separation between the CTM and MTO catalysts by introducing α-Al_2O_3 in the mechanical mixture (DMM in Fig. 2), only minor effects are observed with respect to the undiluted mechanical mixture (MM); the DMM resulted in the lowest CO selectivity (55%) but also in the highest CH_4 and C_{2+} paraffins selectivity (8 and 25%, respectively). This indicates that the beneficial effect of the SAPO-34 proximity is still in place, as the results are much closer to the ones obtained in the case of the mechanical mixture rather than the consecutive bed (compare CB, DMM and MM columns in Fig. 2). We speculate that the different product distribution could be explained by the presence of a mild acidity of the α-Al_2O_3 diluent, as the increased presence of surface acidity can lead to secondary hydrogenations, thus lowering lower olefins selectivity [41]. When considering the RWGS reaction, the Kp/Keq in this case is equal to 0.91. This value is still substantially close to the value of 1, indicating that the reaction is very close to being equilibrated. We explain the small deviation from the equilibrium with the increased selectivity towards methane observed when testing the DMM.

Since a synergistic effect between the catalysts was observed in terms of product distribution, the In_2O_3-ZrO_2 and SAPO-34 were mixed together in a mortar to obtain a more intimate contact between the two phases (IM column in Fig. 2). In this case we obtained very poor results in terms of product selectivity, leading to a CO selectivity of nearly 95% with a selectivity towards C_{1+} products below 1%. Despite the increased contact between the two catalysts that is expected to favor methanol consumption by the zeolite, the obtained result closely resembles those obtained in the case of the consecutive bed configuration, where the system is fully equilibrated. The worsening of the performances as a result of the mortar mixing was also observed by Gao et al. [29], even if to a lower extent. The authors attributed this behavior to the migration of indium followed by its ionic exchange of with zeolite protons, which significantly decreases the number of strongly acidic sites and ultimately leads to a severe deactivation of the MTO functionality [29]. Pore

blockage during the pelletization of the SAPO-34 and In_2O_3-ZrO_2 was also reported in [42] and cannot be ruled out.

3.6. In_2O_3-ZrO_2 to SAPO-34 ratio effect in the mechanical mixture

Given that the most promising performances were obtained by a mechanical mixture of In_2O_3-ZrO_2 and SAPO-34, we decided to vary the relative ratio of the two materials. Considering the In_2O_3-ZrO_2:SAPO-34 1:1 wt ratio as our benchmark, the tests were carried out by keeping constant the amount of In_2O_3-ZrO_2 (and hence the inlet flowrate and the GHSV, as it is defined in this work per gram of In_2O_3-ZrO_2 catalyst only) and varying the amount of zeolite catalyst to obtain In_2O_3-ZrO_2:SAPO-34 ratios equal to 1:0.3 and 1:2. In this way it is possible to vary the contact time over the MTO catalyst while working at constant contact time over the CTM catalyst. The trends of CO_2 conversion and C-selectivity for the three mechanical mixtures are reported Fig. 8 for the first 70 h on stream at 380 °C. The reader is referred to the experimental section for a detailed description of the start-up procedure.

On all mechanical mixtures CO_2 conversion is stable after around 10 h, and then remains constant as the C-containing products rearrange before reaching stability after about 50 h on stream. CO selectivity is initially decreasing, reaches a minimum value when CO_2 conversion is approaching stability and progressively grows at higher ToS. This trend is more pronounced as the amount of SAPO-34 increases in the mechanical mixture, given that CO selectivity is strongly affected by the relative ratio between the CTM and MTO catalysts.

Concerning the C-selectivity towards lower olefins and the corresponding paraffins, some differences can be pointed out as well. In the case of the mechanical mixture with the lower In_2O_3-ZrO_2/SAPO-34 ratio (1:0.3 wt, Fig. 8A) olefins are always produced in higher quantity with respect to paraffins. At the beginning of the test, olefin selectivity goes through a maximum after about 10 h, in correspondence to the minimum CO selectivity. However, the O/P ratio remains very similar throughout the experiment (around 2.7). As the MTO/CTM catalyst ratio increases (In_2O_3-ZrO_2/SAPO-34 wt ratio equal to 1:1 and 1:2 in Figs. 8B and 8C, respectively) the olefin and paraffin selectivity show more marked variations with ToS: not only paraffins are always more abundant than olefins, but in these cases paraffins show a maximum in correspondence to the minimum of CO selectivity. As CO selectivity increases, the olefin and paraffin trends tend to converge, until an O/P ratio approaching 1 in the case of the 1:1 wt mixture (Fig. 8B, ToS = 60 h) and 1.5 in the case of the 1:2 wt mixture (Fig. 8C). In this latter case the maximum in paraffin selectivity is more evident and occurs at the beginning of the run, almost in the absence of olefins production.

In general, it is evident that the initiation of olefin production starts at later ToS as the zeolite load increases. This can be explained by considering that the MTO reaction requires an induction time before becoming effective. In fact, aromatic species need to be formed within the zeolite cages for the MTO reaction to proceed effectively, and by increasing the amount of available zeolite, the time required to accumulate enough aromatics increases.

To compare more effectively the performances of the three mechanical mixtures, the averaged points collected after ToS > 60 h shown in Fig. 8 are compared in Fig. 9.

As previously observed when comparing different arrangements between In_2O_3-ZrO_2 and SAPO-34 in Fig. 6, also in this case all tested mechanical mixtures show minor variations in CO_2 conversion in the presence of significant variations in product selectivity.

Doubling the amount of SAPO-34 (1:2 wt ratio in Fig. 9), causes a marked increase in the amount of C_{2+} hydrocarbons selectivity at the expense of CO selectivity. In these conditions methanol is hardly detected in the condensed products indicating its complete conversion, but the increased SAPO-34 content causes a decrease in the O/P ratio, as most of the produced hydrocarbons are in the form of paraffins. The lower CO and higher hydrocarbon selectivity agrees with the beneficial effect of the methanol removal by the MTO catalyst that we have

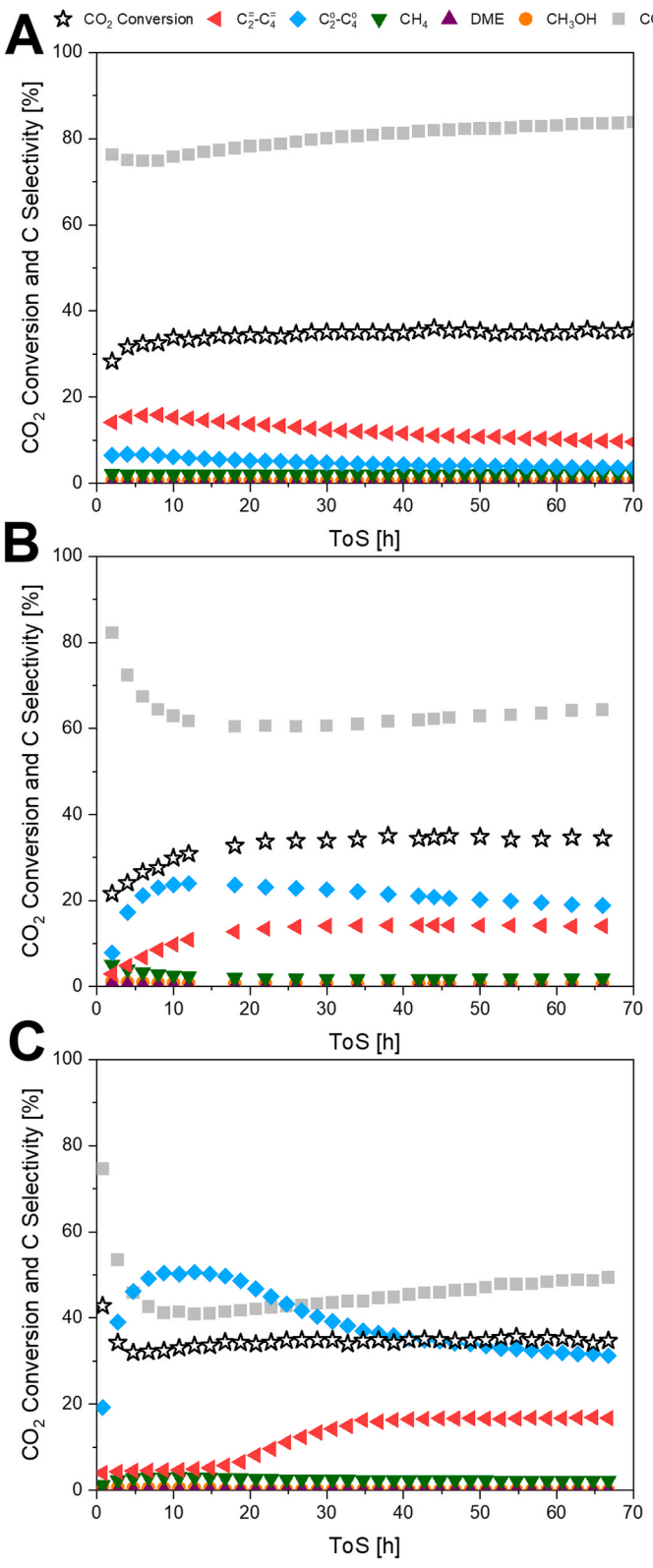

Fig. 8. CO_2 conversion, product selectivity (C-basis) trends as a function of ToS for In_2O_3-ZrO_2/SAPO-34 mechanical mixtures at different In_2O_3-ZrO_2:SAPO-34 wt ratios (A) 1:0.3, B) 1:1, and C) 1:2. Experimental conditions: $H_2/CO_2/Ar$ = 73.5/24.5/2 molar basis, T = 380 °C, P = 38 barg, GHSV = 3 L(STP)/h/g, Flowrate = 6 L(STP)/h.

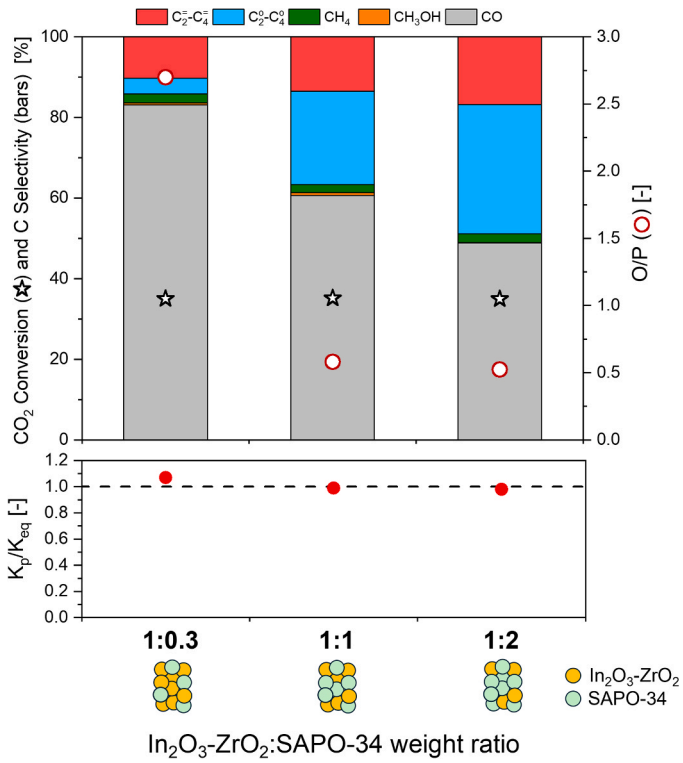

Fig. 9. CO_2 conversion, product selectivity (C-basis) and olefin/paraffin ratio (O/P) on the In_2O_3-ZrO_2/SAPO-34 mechanical mixture at different In_2O_3-ZrO_2: SAPO-34 wt ratios (1:0.3, 1:1, and 1:2, respectively). For each configuration, the ratio between the Kp and Keq of the RWGS equation is also shown. Experimental conditions: $H_2/CO_2/Ar$ = 73.5/24.5/2 molar basis, T = 380 °C, P = 38 barg, GHSV = 3 L(STP)/h/g, Flowrate = 6 L(STP)/h.

previously pointed out in Section 3.5. The increase in lower paraffins selectivity can be attributed to the long residence time on the zeolite in the presence of high H_2 partial pressures [26,43]. The higher paraffin production as the zeolite load increases can be explained both by the accumulation of aromatic species which results in the production of paraffins due to the hydrogen transfer [40], as well as to the occurring of hydrogenation reactions of the produced olefins at higher methanol contact time over the zeolite in the presence of high H_2 partial pressure [12].

Upon decreasing the SAPO-34 content (1:0.3 wt ratio in Fig. 9), the CO selectivity increases to values in excess of 80%. However, olefins are abundant in the hydrocarbon pool, with an O/P ratio in excess of 2.7. By lowering the zeolite mass, in fact, the beneficial effect of methanol removal from the reaction environment decreases, resulting in a lower methanol and hence hydrocarbons production. Lowering the zeolite content in the reactor, however, reduces the contact time over the zeolite catalyst of the produced olefins, resulting in a net increase in lower olefins at the expense of lower paraffins.

Increasing the SAPO-34 content increases the production of hydrocarbons and lowers CO selectivity by effectively shifting the thermodynamic equilibrium by constantly removing methanol from the reaction environment. This effect is able to shift the product distribution, but it cannot increase the CO_2 conversion. This can be explained by invoking once again the complex interplay between two equilibrium-limited reactions (i.e., RWGS and methanol synthesis) and one in kinetic control (i.e., MTO). At the investigated conditions, CH_3OH is constantly removed from the reaction environment by the MTO reaction. At variance, the RWGS reaction is always equilibrated, as shown by its Kp/Keq ratio equal to 1 (Fig. 9). Based on the previous discussion on the 1:1 MM, the kinetics of the RWGS reaction able to restore its equilibrium composition, considering the additional CO and H_2 consumption required to form the extra CH_3OH, as well as the additional H_2O formation coming from the MTO reaction. In other words, CH_3OH consumption is not fast enough compared to the RWGS. With this in mind, it is unsurprising that by lowering the SAPO-34 content CO_2 conversion remains unchanged, as in this way we are decreasing the contact time over the MTO catalyst, and hence the extent of the CH_3OH consumption reaction. It is more surprising that even by doubling the amount of MTO catalyst with the 1:2 mixture, where CH_3OH consumption reaction proceeds faster as indicated by the higher hydrocarbon content, the CO_2 conversion still remains chained to the equilibrium value. By increasing the zeolite content (i.e. increasing CH_3OH removal) at the same process conditions it should be eventually possible to overcome the equilibrium value of ~35%; however, as the zeolite mass increases the MTO reactivity becomes more and more selective towards paraffins thus making the process less appealing.

4. Conclusions

The effect of different In_2O_3-ZrO_2 and SAPO-34 arrangements in the CO_2 to olefins reaction have been investigated in this paper. An intermediate distance between CTM and MTO catalysts, achieved using a mechanical mixture of powdered catalysts, offered promising performances. In fact, when the contact is too intimate or too loose the reaction brings mainly to CO, with paraffins dominating the hydrocarbon pool. The relative amount of In_2O_3-ZrO_2 and SAPO-34 can steer the product selectivity: increasing the quantity of SAPO-34 lowers CO selectivity and enhances MeOH production, leading to higher hydrocarbon yields. However, the longer residence time of the MeOH in the SAPO-34 resulted in a lower O/P. The arrangement and relative ratio of the two catalysts leads to marked differences in the product distribution, but at the investigated process conditions the CO_2 conversion remains constant and limited by the by the RWGS thermodynamic equilibrium.

The characterization of the spent materials after hundreds of hours on stream indicated In_2O_3 sintering on In_2O_3-ZrO_2 and Al and P loss from the SAPO-34, suggesting that both materials need to be improved to withstand the high temperatures and pressure required for the one-pot synthesis. Furthermore, in the case of the spent material from the mechanical mixture, In presence on SAPO-34 crystals was observed, posing concerns to the long-term stability of the catalytic materials in the process.

CRediT authorship contribution statement

Alessandro Porta: Writing - original draft, Writing - review & editing, Conceptualization, Methodology, Investigation, Data curation. **Chiara Coffano**: Writing – original draft, Investigation, Data curation, Conceptualization. **Mattia Piacentini**: Writing – review & editing, Investigation. **Francesca Rabino**: Writing – review & editing, Supervision, Project administration. **Barbara Picutti**: Project administration, Methodology. **Luca Lietti**: Writing – review & editing, Project administration, Methodology, Funding acquisition. **Carlo Giorgio Visconti**: Writing – review & editing, Supervision, Project administration, Funding acquisition, Conceptualization.

Declaration of Competing Interest

The authors declare that they have no known competing financial interests or personal relationships that could have appeared to influence the work reported in this paper.

Data Availability

The authors do not have permission to share data.

Appendix A. Supporting information

Supplementary data associated with this article can be found in the online version at doi:10.1016/j.apcata.2024.119799.

References

[1] G.A. Olah, A. Goeppert, G.K.S. Prakash, J. Org. Chemi 74 (2009) 487–498.
[2] E.A. Quadrelli, G. Centi, J.L. Duplan, S. Perathoner, ChemSusChem 4 (2011) 1194–1215.
[3] G. Centi, E.A. Quadrelli, S. Perathoner, Energy Environ. Sci. 6 (2013) 1711–1731.
[4] G. Collodi, G. Azzaro, N. Ferrari, S. Santos, Energy Procedia 114 (2017) 122–138.
[5] R.M. Cuéllar-Franca, A. Azapagic, *J. CO_2 Util.* 9 (2015) 82–102.
[6] H.M. Torres Galvis, K.P. De Jong, ACS Catal. 3 (2013) 2130–2149.
[7] D. Gao, W. Li, H. Wang, G. Wang, R. Cai, *Trans. Tianjin Univ.* 2022 28 4 (28) (2022) 245–264.
[8] T.P. Araújo, A. Shah, C. Mondelli, J.A. Stewart, D. Curulla Ferré, J. Pérez-Ramírez, Appl. Catal. B: Environ. 285 (2021) 119878.
[9] A. Portillo, O. Parra, A.T. Aguayo, J. Ereña, J. Bilbao, A. Ateka, ACS Sustain Chem. Eng. 12 (2024) 1616–1624.
[10] D. Cai, Y. Cai, K.B. Tan, G. Zhan, *Mater.* 2023 16 (2023) 2803.
[11] S.S. Arora, A. Bhan, J. Catal. 356 (2017) 300–306.
[12] S.S. Arora, Z. Shi, A. Bhan, ACS Catal. 9 (2019) 6407–6414.
[13] M. Ronda-Lloret, G. Rothenberg, N.R. Shiju, ChemSusChem 12 (2019) 3896–3914.
[14] O. Martin, A.J. Martín, C. Mondelli, S. Mitchell, T.F. Segawa, R. Hauert, C. Drouilly, D. Curulla-Ferré, J. Pérez-Ramírez, Angew. Chem. Int Ed. 55 (2016) 6261–6265.
[15] D. Wang, Z. Xie, M.D. Porosoff, J.G. Chen, Chem 7 (2021) 2277–2311.
[16] M. Bowker, ChemCatChem 11 (2019) 4238–4246.
[17] A. Portillo, A. Ateka, J. Ereña, J. Bilbao, A.T. Aguayo, J. Environ. Manag. 316 (2022) 115329.
[18] F. Salomone, E. Sartoretti, S. Ballauri, M. Castellino, C. Novara, F. Giorgis, R. Pirone, S. Bensaid, Catal. Today 423 (2023) 114023.
[19] M.S. Frei, C. Mondelli, A. Cesarini, F. Krumeich, R. Hauert, J.A. Stewart, D. Curulla Ferré, J. Pérez-Ramírez, ACS Catal. 10 (2020) 1133–1145.
[20] S.S. Arora, D.L.S. Nieskens, A. Malek, A. Bhan, *Nat. Catal.* 2018 1 9 (1) (2018) 666–672.
[21] U. Olsbye, S. Svelle, M. Bjrgen, P. Beato, T.V.W. Janssens, F. Joensen, S. Bordiga, K. P. Lillerud, Angew. Chem. Int Ed. 51 (2012) 5810–5831.
[22] J. Xie, D.S. Firth, T. Cordero-Lanzac, A. Airi, C. Negri, S. Øien-Ødegaard, K. P. Lillerud, S. Bordiga, U. Olsbye, ACS Catal. 12 (2022) 1520–1531.
[23] X. Zhao, J. Li, P. Tian, L. Wang, X. Li, S. Lin, X. Guo, Z. Liu, ACS Catal. 9 (2019) 3017–3025.
[24] S. Dang, P. Gao, Z. Liu, X. Chen, C. Yang, H. Wang, L. Zhong, S. Li, Y. Sun, J. Catal. 364 (2018) 382–393.
[25] W. Zhang, S. Wang, S. Guo, Z. Qin, M. Dong, J. Wang, W. Fan, J. Catal. 413 (2022) 923–933.
[26] C. Coffano, A. Porta, C.G. Visconti, F. Rabino, G. Franzoni, B. Picutti, L. Lietti, Catal. Today 418 (2023) 114133.
[27] I.J. Castellanos-Beltran, G.P. Assima, J.M. Lavoie, Front Chem. Sci. Eng. 12 (2018) 226–238.
[28] L. Zhang, Z. Cao, Z. Gao, W. Liu, Y. Mao, M. Li, H. Peng, Ind. Eng. Chem. Res 62 (2023) 9123–9133.
[29] P. Gao, S. Dang, S. Li, X. Bu, Z. Liu, M. Qiu, C. Yang, H. Wang, L. Zhong, Y. Han, Q. Liu, W. Wei, Y. Sun, ACS Catal. 8 (2018) 571–578.
[30] S.A. Chernyak, M. Corda, M. Marinova, O.V. Safonova, V.A. Kondratenko, E. V. Kondratenko, Y.G. Kolyagin, K. Cheng, V.V. Ordomsky, A.Y. Khodakov, ACS Catal. 13 (2023) 14627–14638.
[31] L. Zhang, B. Geng, P. Wang, H. Kang, H. Xiao, J. Jia, H. Wu, Appl. Catal. A Gen. 657 (2023) 119141.
[32] Y. Shi, W. Gao, G. Wang, J. Fan, C. Wang, F. Wang, Y. He, X. Guo, S. Yasuda, G. Yang, N. Tsubaki, Mater. Today Chem. 32 (2023) 101654.
[33] S. Tada, D. Li, M. Okazaki, H. Kinoshita, M. Nishijima, N. Yamauchi, Y. Kobayashi, K. Iyoki, Catal. Today 411–412 (2023) 113828.
[34] T. Xie, J. Ding, X. Shang, X. Zhang, Q. Zhong, J. Colloid Interface Sci. 635 (2023) 148–158.
[35] Y. Ding, F. Jiao, X. Pan, Y. Ji, M. Li, R. Si, Y. Pan, G. Hou, X. Bao, ACS Catal. 11 (2021) 9729–9737.
[36] Y. Wang, G. Wang, L.I. van der Wal, K. Cheng, Q. Zhang, K.P. de Jong, Y. Wang, Angew. Chem. Int Ed. 60 (2021) 17735–17743.
[37] M. Zhang, S. Xu, Y. Wei, J. Li, J. Wang, W. Zhang, S. Gao, Z. Liu, Chin. J. Catal. 37 (2016) 1413–1422.
[38] R. Vomscheid, M. Briend, M.J. Peltre, P. Massiani, P.P. Man, D. Barthomeuf, J. Chem. Soc. Chem. Commun. (1993) 544–546.
[39] F.D.P. Mees, L.R.M. Martens, M.J.G. Janssen, A.A. Verberckmoes, E.F. Vansant, Chem. Comm. (2003) 44–45.
[40] S. Müller, Y. Liu, F.M. Kirchberger, M. Tonigold, M. Sanchez-Sanchez, J.A. Lercher, J. Am. Chem. Soc. 138 (2016) 15994–16003.
[41] J. Kanai, J.A. Martens, P.A. Jacobs, J. Catal. 133 (1992) 527–543.
[42] A. Portillo, O. Parra, A.T. Aguayo, J. Ereña, J. Bilbao, A. Ateka, Catalysts 13 (2023) 1101.
[43] R.B. Rostami, A.S. Lemraski, M. Ghavipour, R.M. Behbahani, B.H. Shahraki, T. Hamule, Chem. Eng. Res Des. 106 (2016) 347–355.